the plant journal

SEB SOCIETY FOR EXPERIMENTAL BIOLOGY

The Plant Journal (2020) **104,** 839–855 doi: 10.1111/tpj.14956

TECHNICAL ADVANCE

Rapid temperature responses of photosystem II efficiency forecast genotypic variation in rice vegetative heat tolerance

John N. Ferguson[1,2,*], Lorna McAusland[1], Kellie E. Smith[1], Adam H. Price[3], Zoe A. Wilson[1] and Erik H. Murchie[1]

[1]*Division of Plant and Crop Science, School of Biosciences, University of Nottingham, Sutton Bonington Campus, Sutton Bonington, Leicestershire LE12 5RD, UK,*

[2]*Future Food Beacon of Excellence, University of Nottingham, Sutton Bonington Campus, Leicestershire LE12 5RD, UK, and*

[3]*School of Biological Sciences, University of Aberdeen, Aberdeen AB24 3UU, UK*

Received 15 April 2020; revised 22 June 2020; accepted 22 July 2020; published online 10 August 2020.

*For correspondence (e-mails john.ferguson@nottingham.ac.uk or johnferguson1989@gmail.com).

SUMMARY

A key target for the improvement of *Oryza sativa* (rice) is the development of heat-tolerant varieties. This necessitates the development of high-throughput methodologies for the screening of heat tolerance. Progress has been made to this end via visual scoring and chlorophyll fluorescence; however, these approaches demand large infrastructural investments to expose large populations of adult plants to heat stress. To address this bottleneck, we investigated the response of the maximum quantum efficiency of photosystem II (PSII) to rapidly increasing temperatures in excised leaf segments of juvenile rice plants. Segmented models explained the majority of the observed variation in response. Coefficients from these models, i.e. critical temperature (T_{crit}) and the initial response (m_1), were evaluated for their usability for forecasting adult heat tolerance, measured as the vegetative heat tolerance of adult rice plants through visual (stay-green) and chlorophyll fluorescence (ϕPSII) approaches. We detected substantial variation in heat tolerance of a randomly selected set of *indica* rice varieties. Both T_{crit} and m_1 were associated with measured heat tolerance in adult plants, highlighting their usability as high-throughput proxies. Variation in heat tolerance was associated with daytime respiration but not with photosynthetic capacity, highlighting a role for the non-photorespiratory release of CO_2 in heat tolerance. To date, this represents the first published instance of genetic variation in these key gas-exchange traits being quantified in response to heat stress in a diverse set of rice accessions. These results outline an efficient strategy for screening heat tolerance and accentuate the need to focus on reduced rates of respiration to improve heat tolerance in rice.

Keywords: chlorophyll fluorescence, stay-green, photosynthesis, heat stress, *Oryza sativa*, high-throughput phenotyping, technical advance.

INTRODUCTION

Global climatic change is a key contributor to the multifaceted challenge of achieving food security. The increase in average Earth surface temperatures is a fundamental aspect of climate change and is well understood to be particularly detrimental to agricultural productivity. In concurrence, independent model estimates have indicated that with each incremental increase in surface temperature (per °C) there are concurrent decreases in rice yields of up to 3.2% (Zhao *et al.*, 2017). Moreover, empirical evidence from field-based temperature manipulation studies have demonstrated that an increase in air temperature of approximately 3°C can significantly reduce carbon fixation and grain yield (Chaturvedi *et al.*, 2017). When this evidence is taken in the context of the forecasted increases in average surface temperatures of 0.2°C per decade (IPPC, 2007), it is evident that the development of elite rice varieties that produce stable yields during heat stress events is a key priority for future crop improvement.

Heat stress upregulates the expression of intrachloroplastic proteases that perturb chloroplast structure and function through protein degradation (Sinvany-Villalobo *et al.*, 2004). The degradation of Rubisco and other proteins involved in carbon fixation with intensifying temperatures reduces photosynthesis (Jagadish *et al.*, 2015; Chen *et al.*, 2019). As photosynthesis is the ultimate basis of yield (Zhu

et al., 2010), reductions herein are of critical importance for crop production. Prolonged instances of temperatures above optimal for typical plant functionality disrupt photosynthetic carbon fixation. This disruption of photosynthesis commonly co-occurs with early-onset and accelerated leaf senescence, which results from chlorophyll degradation caused by reactive oxygen species (ROS; Khanna-Chopra, 2012; Jajic *et al*., 2015), as well as through vacuolar collapse and the disruption of cellular homeostasis (Lim *et al*., 2007; Cossani and Reynolds, 2012). These processes are developmentally pre-programmed to initiate and control senescence during reproductive growth (Sekhon *et al*., 2019). Delayed and/or reduced senescence is typically referred to as 'stay green' (SG). SG is recognized as a key physiological trait and physical marker for stress adaptation, as it permits the maintenance of photosynthesis (Lim *et al*., 2007). Furthermore, as SG can be evaluated rapidly across a population, it has been phenotypically and genetically linked to yield in key crops, such as *Triticum aestivum* (wheat; Kumar *et al*., 2010; Vijayalakshmi *et al*., 2010), *Sorghum bicolor* (sorghum; Rama Reddy *et al*., 2014) and *Oryza sativa* (rice; Yoo *et al*., 2007; Fu *et al*., 2011). Despite this link, it is important to note that the developmental timing of reductions in foliar carbon fixation and concurrent senescence can define yield consequences. For example, senescence triggered or accelerated by heat stress during grain filling is typically important for stabilizing yield, as it facilitates the remobilization of carbon from vegetative sources or stores to reproductive sinks (Uauy *et al*., 2006). Selection on SG pre-anthesis, and sometimes during and post-anthesis, can afford yield benefits under heat stress, however, through the assimilation of extra photosynthates that are directly translocated to reproductive processes or are stored as water-soluble carbohydrates in the stem and subsequently remobilized (Blum, 2009; Jagadish *et al*., 2015).

Heat stress is also particularly damaging to the oxygen-evolving complex of photosystem II (PSII), the initial site of light-dependent photosynthetic reactions (Murata *et al*., 2007). The repair mechanism of PSII is inhibited by heat-induced ROS production, leading to increased photoinhibition, which impairs photosynthesis (Allakhverdiev *et al*., 2008). PSII efficiency can be quantified *in vivo* through chlorophyll fluorescence techniques (Baker, 2008), where the associated methodologies are relatively accessible and can provide a general measure of the photosynthetic response to stress (Murchie *et al*., 2018). The usefulness of chlorophyll fluorescence for understanding crop heat tolerance has been successfully employed in a series of studies focusing on natural variation in wheat (Sharma *et al*., 2012, 2015; Sharma *et al*., 2017). In these studies, the response of the maximum quantum efficiency of PSII (F_v/F_m) to heat stress was observed to correlate with traits linked to heat tolerance, such as chlorophyll content and biomass accumulation after heat stress (Sharma *et al*., 2015). Subsequently, genetic loci underlying variation in the response of F_v/F_m to heat stress were detected through quantitative trait loci (QTLs) mapping, and were observed to co-localize with known heat-tolerance genes (Sharma *et al*., 2017).

Introducing and developing heat tolerance into modern germplasm requires the ability to screen large populations of natural genotypes, or mutants, for breeding or forward-genetic screens (Driedonks *et al*., 2016). Visual assessments of SG or measurements of chlorophyll fluorescence are somewhat amenable to this end, as they are relatively quick, do not require expensive equipment and provide a good indication of the maintenance of carbon fixation and heat tolerance that can be associated with yield. As physical markers of heat tolerance they can be limiting, however, in that they require substantial infrastructure investment, such as facilities to induce heat stress or access to multiple field sites to leverage naturally occurring heat stress. Additionally, adequate space to grow plants to adult and reproductive developmental stages can be substantially limiting. For example, Sharma *et al.* (2012) required considerable glasshouse and climate chamber space in order to quantify the heritable variation of the heat response of F_v/F_m in a panel of over 1200 wheat varieties at adult developmental stages. Consequently, employing SG or chlorophyll fluorescence as physical markers for selection can represent a phenotyping bottleneck for adapting crops to future environments.

With this study we sought to develop a novel and rapid methodology for understanding the temperature response of PSII photochemistry. Through broken-line analyses we hypothesized that it would be possible to accurately characterize this response and that this characterization could be used to forecast the heat tolerance of foliar tissue, through the relationship between the maintenance of photosynthesis under heat stress and SG. Consequently, we tested the efficiency of the initial response of F_v/F_m to temperature and the critical temperature of F_v/F_m in excised juvenile tissue segments for predicting SG in adult plants. Finally, we explored how this related to traditional metrics of photosynthetic responses to heat stress, demonstrating the first published example of the assessment of the genetic variation of key photosynthetic traits in response to heat stress in rice to date.

RESULTS

Genotypic variation in the response of excised juvenile leaf segments to rapidly increasing temperatures

A small portion of leaf tissue was excised from the youngest leaf of 10-day-old rice plants in order to measure F_v/F_m at incrementally increasing temperatures (approx. 21–50°C) within a closed chlorophyll fluorescence system

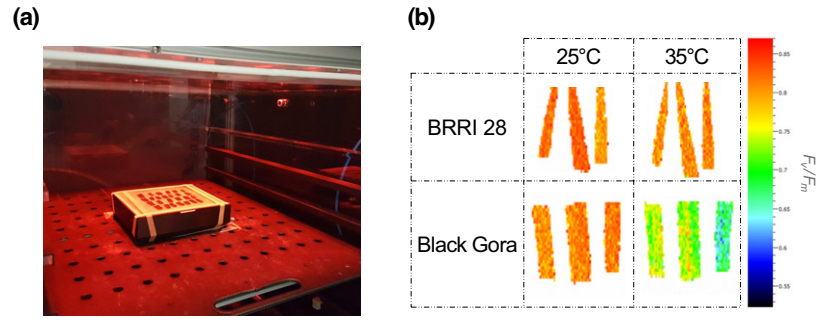

Figure 1. (a) Experimental set-up showing leaf segments encased between glass plates inside the fluorcam imaging platform under actinic light. After chlorophyll fluorescence measurements at each temperature, the glass plates are removed and submerged within plastic bags into a pre-set water bath for the period of time required to reach subsequent temperatures. (b) Variation in maximum quantum efficiency of photosystem II (F_v/F_m) of the same three biological repeats of two genotypes (BRR 28 and Black Gora) after incubation in the water bath at 25 and 35°C.

(Figure 1a). This allowed for the detection of genotypic variation in minimum chlorophyll fluorescence (F_o) and F_v/F_m at multiple temperatures (Figures 1b and 2a,b). In general, all seven genotypes demonstrated the same trend of an exponential increase in F_o, where small increases were induced by the initial lower temperatures and rapid increases were induced by the higher temperatures (Figure 2a). The response of F_o to temperature was reflected by F_v/F_m, where all genotypes demonstrated a response to temperature similar to a logistic decay (Figure 2b). We tested whether the process of removing the plant material encased in glass plates into and out of a water bath before measuring chlorophyll fluorescence impacted the values of F_o and F_v/F_m, irrespective of temperature changes, but noted no change in either parameter when performing the regular experimental procedure without incremental temperature changes (Figure S1).

At the initial temperatures there was little variation in chlorophyll fluorescence between the genotypes (Figure 2a,b). As temperatures increased, significant genetic variation was detected: for example, F_v/F_m at 35°C varied from 0.62 for Black Gora (SE = 0.03) to 0.80 for BJI (SE = 0.00). A repeated-measures one-way analysis of variance (ANOVA) demonstrated that there were significant genotype and temperature effects on both F_o and F_v/F_m (Figure 2a,b). Additionally, a significant interaction between genotype and temperature was detected (Figure 2a,b), suggesting that genotype differences in fluorescence parameters were dependent on temperature. This is evident when comparing the F_o response to temperature of IR 64: for example, IR 64 had the highest value of all genotypes at 30°C (149.14; SE = 11.42) but the lowest value at 48°C (262.05; SE = 10.51). A similar effect is seen with the BJI genotype and the F_v/F_m parameter, where BJI demonstrated the highest value of all genotypes at 30°C (0.81; SE = 0.00) but the second lowest value at 48°C (0.04; SE = 0.02).

We modelled the response of F_v/F_m to temperature of each individually excised leaf segment through a linear model and a quadratic model. The coefficient of determination (R^2) of the linear models varied moderately within genotypes, where within-genotype standard errors ranged from 0.02 to 0.05, suggesting that linear models do not describe the relationship between F_v/F_m and temperature in a wholly consistent manner (Figure 3). Moreover, the variation in the linear model R^2 between genotypes was significantly different ($P < 0.01$), where the mean ranged from 0.57 to 0.81 (Figure 3), thereby indicating that linear models are better at describing this relationship for certain genotypes than others. Conversely, intragenotypic variation in the R^2 values of quadratic models varied little, where within-genotype standard errors were consistently ≤0.01 (Figure 3). Furthermore, the variation between genotypes for R^2 varied much less for quadratic than linear models, where the lowest genotype mean value was 0.91 and the highest was 0.96. This still represented a significant difference according to a one-way ANOVA, however (P <0.01; Figure 3).

The fitted linear models were used to produce segmented models through broken-line analyses (see 'Experimental procedures'). Segmented models out-performed linear and quadratic models with respect to minimizing intra- and intergenotypic variation (Figure 3). The within-genotype standard errors of R^2 were <0.00 for all genotypes, and the genotype mean values varied from 0.97 to 0.99 ($P = 0.06$). Therefore, this suggests that segmented models do not bias certain genotypes in their modelling of the response of F_v/F_m to temperature to the same extent as linear or quadratic models.

Fitting segmented models to the response of F_v/F_m to temperature allowed us to characterize this relationship in three ways. For all individual models only one breakpoint in the relationship was ever detected. We term this so-called breakpoint as the critical temperature of F_v/F_m (T_{crit}), as it defines the temperature point at which F_v/F_m transitions from a slow to a rapid decline (Figure 2c). Genotype mean values for T_{crit} varied from 36.48°C (SE = 1.18°C) for

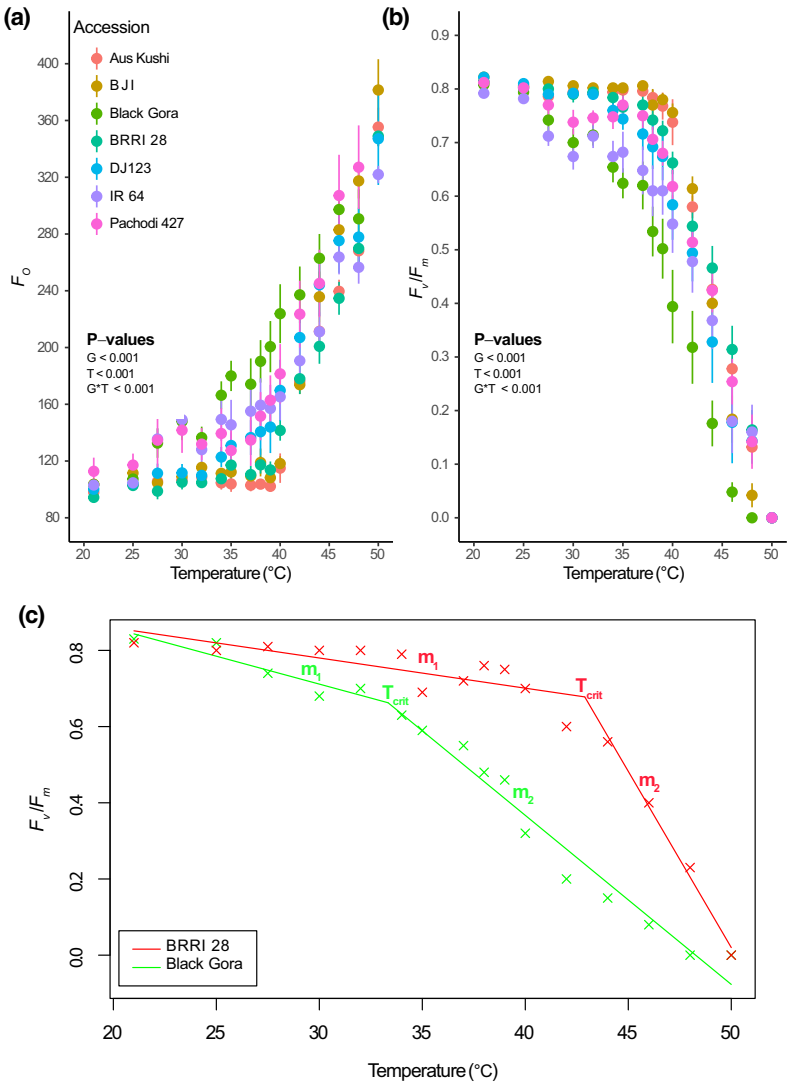

Figure 2. The response of key chlorophyll fluorescence parameters to incrementally increasing temperatures. (a) The response of minimum chlorophyll fluorescence (F_o) to increasing temperatures in the seven genotypes. (b) The response of the maximum quantum efficiency of photosystem II (F_v/F_m) to increasing temperatures in the seven genotypes. (a–b) Filled circles denote the mean of each genotype and error bars denote the standard error of the mean. The *P* values of all terms – genotype (G) and temperature (T) – from a one-way repeated measures analysis of variance are inset. (c) Example of the segmented analyses used to assess the response of F_v/F_m to temperature. The crosses represent individual data points of F_v/F_m at all temperatures measured for a single biological repeat of BRRI 28 (red) and Black Gora (green). The solid lines represent the segmented models that describe the response of F_v/F_m to temperature for each biological repeat.

Black Gora to 39.89°C (SE = 0.32°C) for BJI (Figure 4a). The slopes of the linear regressions fitted before and after T_{crit} were extracted and designated as m_1 and m_2, respectively. m_1 and m_2 define the strength of the relationship of F_v/F_m and temperature before and after T_{crit}. The genotype mean values of m_1 varied from 0.0008 (SE = 0.0001) for Aus Kushi to 0.0125 (SE = 0.0016) for Black Gora (Figure 4b). A linear model regressing T_{crit} on m_1 demonstrated a negative relationship between the two parameters (Figures 4d and 5; Table S1), where the lines that respond more strongly to initial temperature changes had the lowest T_{crit}. Genotype means for m_2 varied from 0.051 (SE = 0.008) for Black Gora to 0.088 (SE = 0.006) for BJI (Figure 4c). T_{crit} and m_2 did not show a discernible association (Figure 5; Table S1); however, m_1 and m_2 demonstrated a significant negative association, suggesting that the lines that respond most strongly to temperature before T_{crit} respond least strongly after T_{crit}, and vice versa (Figure 5; Table S1).

Genotypic variation in vegetative heat tolerance in adult plants

We subjected adult plants to an 8-day-long period of heat stress (42°C day temperature) at 60 days post sowing. At this point, the majority of plants were transitioning from the tillering to the stem elongation growth stage (Lancashire *et al.*, 1991). This stage was chosen because of the importance of the heat tolerance of foliar tissue and the maintenance of photosynthesis just prior to reproductive growth (Jagadish *et al.*, 2015). During the heat-stress period, the operational efficiency of PSII in light (ϕPSII) was assessed every day to determine the impact of heat stress on the photosynthetic biochemistry of all genotypes (Figures 6 and S3). ϕPSII decreased across the duration of the heat-stress period for all genotypes except BRRI 28. The most substantial reductions were observed from 6 days after heat-stress initiation (Figure S3). We calculated the percentage reduction in ϕPSII from day 1 to day 8 of the heat-stress experiment (Figure S3). BRRI 28 did not

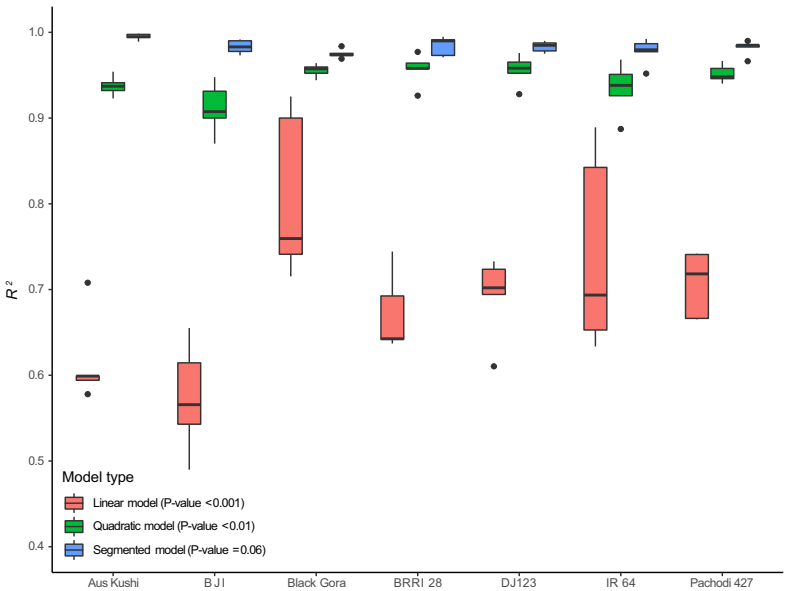

Figure 3. Effectiveness of the broken-line analyses for describing the relationship between the maximum efficiency of photosystem II (F_v/F_m) and temperature. Box plots describe the variation in the coefficient of determination (R^2) of models – linear (red), quadratic (green) and segmented (blue) – that predict F_v/F_m from temperature for each genotype. Each box plot denotes the interquartile range (IQR; 25th–75th percentile), with the 50th percentile marked. The whiskers extend to maximum values within 1.5 times the IQR, with values outside of this range being indicated by black dots. The *P* values from a one-way analysis of variance describing R^2 as a function of genotype for each model are indicated within parentheses in the inset legend.

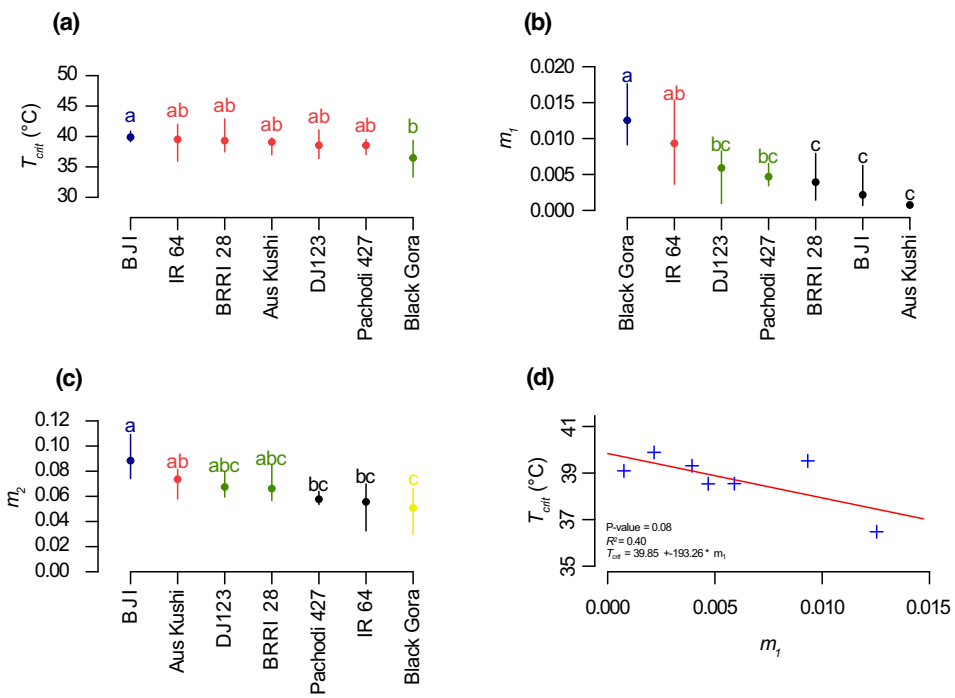

Figure 4. Characterization of the response of maximum quantum efficiency of photosystem II (F_v/F_m) to temperature in the seven genotypes. (a–c) Dot plots demonstrating the variation in the critical temperature (T_{crit}) of F_v/F_m (a), the initial rate of response of F_v/F_m to increasing temperature (m_1, b) and the secondary rate of response of F_v/F_m to increasing temperature (m_2, c). Individual dots represent means of each genotype and error bars extend to the maximum and minimum value. Statistically significant differences between genotypes are denoted by different colours and by different letter groups above each genotype. (d) The relationship between m_1 and T_{crit}. The blue crosses indicate individual data points and the linear regression for T_{crit} as a function of m_1 is denoted by the solid red line. The associated *P* value and R^2 value of the linear model are inset.

respond to heat stress in terms of ϕPSII (Figures 6 and S3), indeed ϕPSII actually increased marginally during this period for BRRI 28, yielding a negative percentage decrease (Figure S3d). The remainder of the genotypes showed significant reductions in ϕPSII, leading to a range in percentage declines from 8.06 for IR 64 to 34.59 for Black Gora (Figure S3).

After 7 days from heat-stress initiation, SG was visually scored as the stay-green rating (SGR) on all plants. SGR describes the extent of fully expanded foliar tissue that is senesced and varies from 1 (no senescence) to 5 (total leaf and stem death). Genotype means of SGR varied from 1.50 (SE = 0.29) for BRRI 28 to 3.75 (SE = 0.25) for Black Gora. Four statistically significant different genotype groups were established for SGR (Figure 7a).

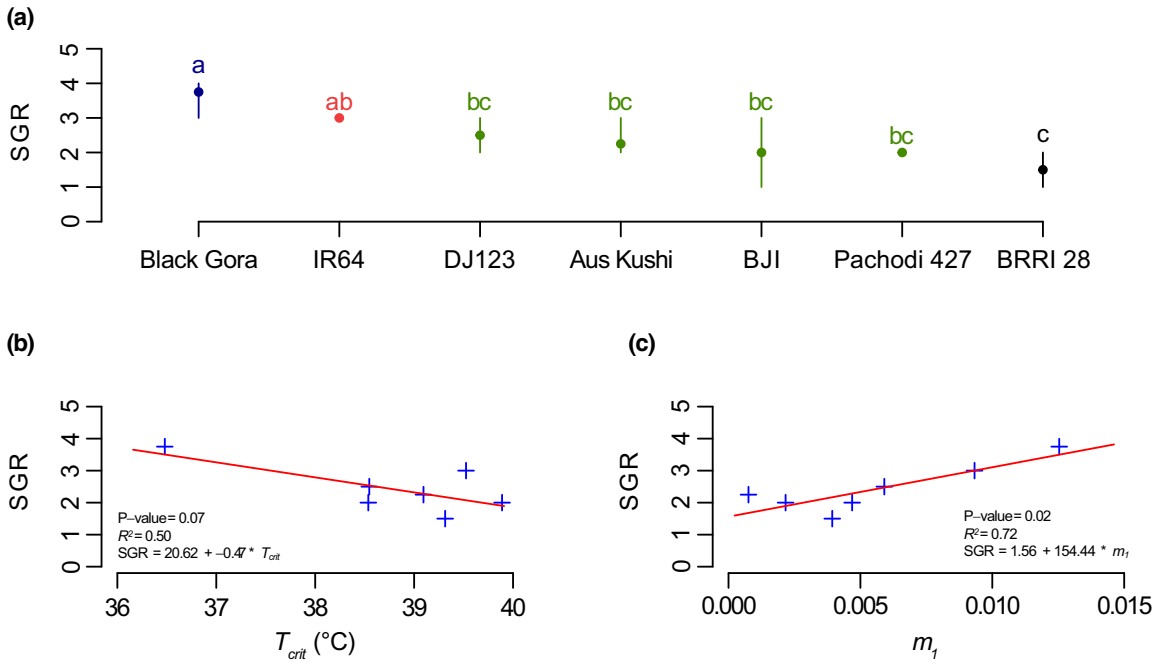

Figure 5. (a) Variation in the visual scoring of the stay-green rating (SGR) of the seven genotypes. Individual dots represent means of each genotype and the error bars extend to the maximum and minimum values. Statistically significant differences between genotypes are denoted by different colours and by different letter groups above each genotype. (b) The relationship between T_{crit} and SGR. The linear model regressing SGR on T_{crit} is denoted by the solid red line. The associated *P* value and R^2 value of the linear model are inset. (c) The relationship between m_1 and SGR. The linear model regressing SGR on m_1 is denoted by the solid red line. The associated *P* value and R^2 value of the linear model are inset.

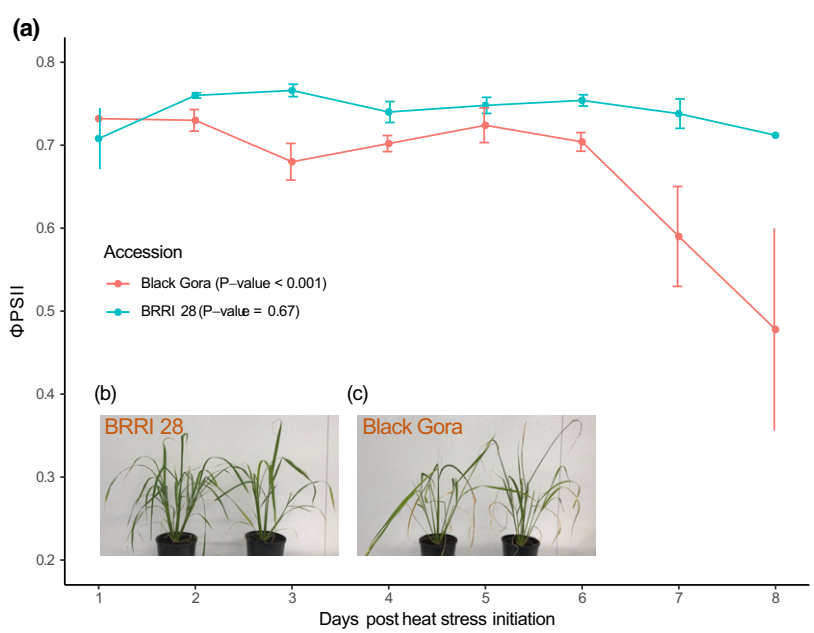

Figure 6. The response of Black Gora and BRRI 28 to 7 days of heat stress. (a) Dot and line plot showing the operating efficiency of photosystem II photochemistry (ΦPSII) every day at midday during the heat-stress period. Each filled circle denotes the genotype mean and the error bars denote the standard error of the mean. (b) Two representative plants of BRRI 28 following 5 days of heat stress. (c) Two representative plants of Black Gora following 5 days of heat stress.

Temperature driven plasticity of photo-physiological traits

We measured the response of net photosynthesis (A_n) to incrementally increasing intracellular CO_2 concentrations (c_i) for all genotypes 3 days before and 5 days after heat-stress initiation. This allowed us to model the maximum rate of carboxylation by Rubisco (V_{cmax}) and the maximum rate of electron transport for RuBP regeneration (J_{max}). These parameters reflect the CO_2-limited and electron transport-limited rates of photosynthesis, respectively. We also calculated the ratio J_{max}:V_{cmax} to provide information on electron usage per Rubisco carboxylation event. Additionally, A_n–c_i response measurements were used to model

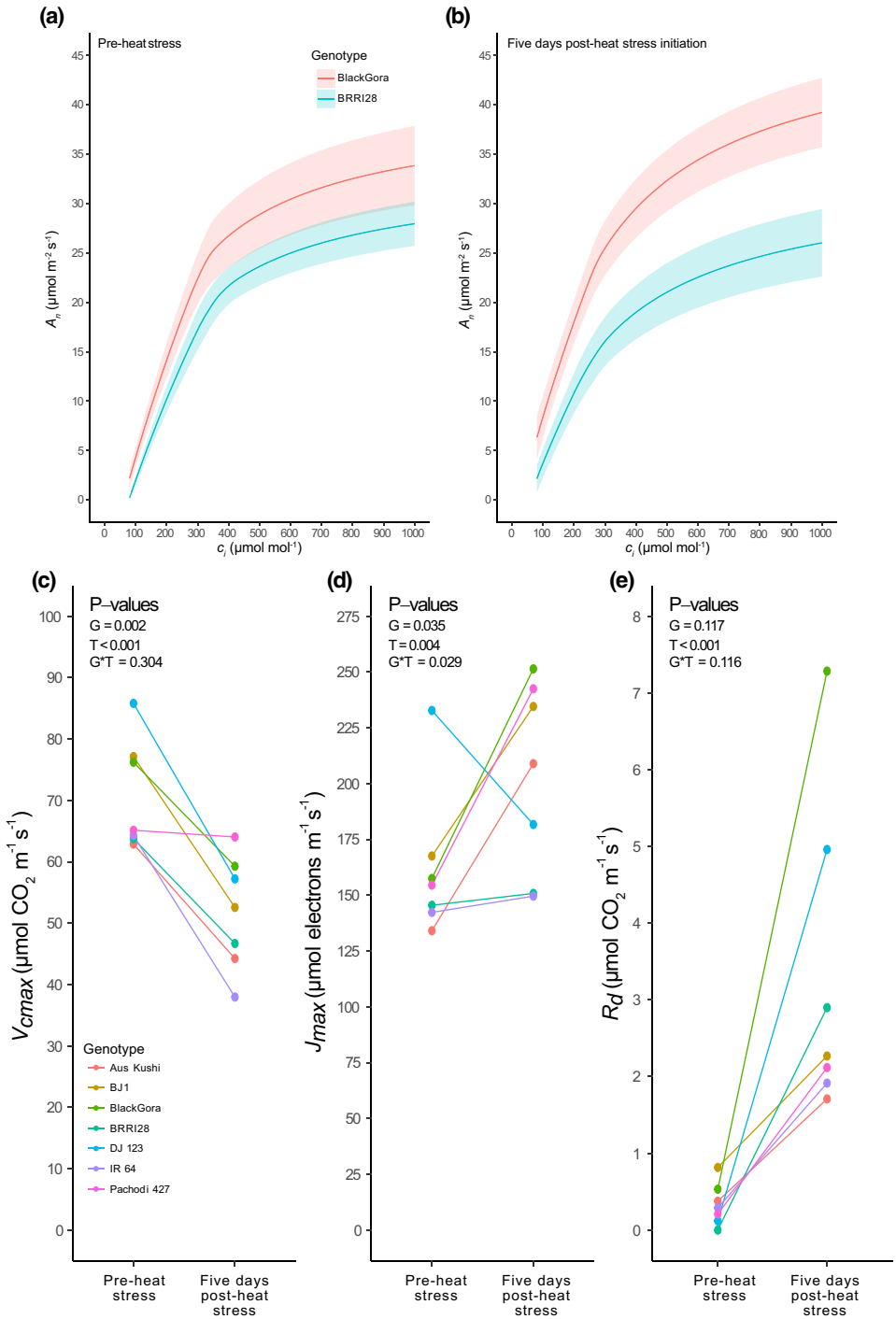

Figure 7. (a–b) The response of net photosynthesis (A_n) to incrementally increasing intracellular carbon dioxide concentrations (c_i) in Black Gora and BRRI 28 before heat stress (a) and 5 days after heat-stress initiation (b). Solid lines represent average A_n values at 50–1000 c_i, according to the Farquhar *et al.* (1980) photosynthesis model. The shaded areas represent the standard error of the mean. (c–e) The response of parameters derived from A_n–c_i response measurements to heat stress for all genotypes. (c) The response of the maximum rate of carboxylation of Rubisco (V_{cmax}). (b) The response of the maximum potential electron transport rate (J_{max}). (c) The response of daytime respiration (R_d). Individual dots represent mean values. *P* values from two-way analyses of variances are inset.

daytime respiration (R_d) as non-photorespiratory release of CO_2 (Figure 8a,b).

Significant variation was detected in V_{cmax} between pre- and post-heat-stress initiation (Figures S4a and S5a). Heat stress was also observed to have a significant impact on V_{cmax}, reducing rates substantially in all genotypes except Pachodi 427 (Figure 8c). Heat stress did not alter the rank order of genotypes for V_{cmax} significantly, as no

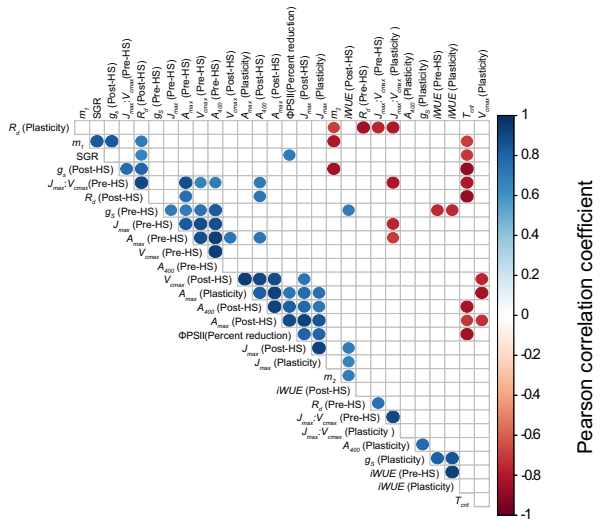

Figure 8. Corrplot describing correlations between all measured traits. All associations where the *P* value from a pairwise test of association is ≤0.1 are indicated by a coloured circle. The colour of the circle indicates the Pearson product–moment correlation coefficient (*r*). Traits measured before and during the heat stress are designated as pre- or post-HS and the plasticity of those traits is also included. Table S1 lists the *P* and *r* values for each pairwise trait interaction.

genotype × temperature (G × T) interaction was identified (Figure 8c). Rates of J_{max} also varied significantly between genotypes before and after heat-stress initiation (Figures S4b and S5b). The heat-stress period had a significant impact on J_{max}, with rates increasing substantially for the majority of genotypes, except for IR 64 and BRRI 28 where only minor increases were noted. Conversely, the J_{max} of DJ 123 showed the opposing response to heat stress and decreased. A significant G × T interaction was observed for J_{max}. The J_{max}:V_{cmax} ratio demonstrated very little variation before and after heat-stress initiation (Figures S4d and S5d), but was upregulated significantly under heat stress in all genotypes without demonstrating any G × T interaction (Figure S6a).

When testing the variation for R_d before and after heat-stress initiation separately, significant genotypic variation was detected (Figures S4c and S5c). Combining this variation into a multiple test demonstrated marginally insignificant genetic variation with no G × T interaction, however, but heat stress was observed to increase the rate of R_d significantly in all genotypes (Figure 8e).

With respect to the non-modelled photo-physiological parameters, only intrinsic water-use efficiency (*iWUE*) demonstrated a significant response to heat stress (Figure S6), and this was primarily associated with the >50% reduction experienced by IR 64 (Figure S6e). In concurrence, *iWUE* was the only parameter herein where a significant G × T interaction was observed (Figure S6).

We calculated the plasticity of photo-physiological traits using the phenotypic plasticity index (PPI) in order to gauge the response of these traits to 5 days of heat stress, where values close to 0 denote a lack of response and values close to 1 denote a strong response. The non-modelled metrics of photosynthetic assimilation of CO_2 demonstrated the lowest phenotypic plasticity for all genotypes, where plasticity for A_{400} ranged from 0.03 to 0.19 (Figure S7e) and plasticity for A_{max} ranged from 0.02 to 0.23 (Figure S7f), suggesting a relatively reduced response to temperature of instantaneous rates of photosynthesis. Conversely, when focusing on particular photosynthetic processes, the modelled rates of V_{cmax} and J_{max} demonstrated much higher degrees of phenotypic plasticity, ranging between 0.01 and 0.41 (Figure S7a) and between 0.04 and 0.37 (Figure S7b), respectively. The final trait modelled from A_n–c_i response measurements, R_d, demonstrated by far the greatest plasticity to heat stress, where the phenotypic plasticity index ranged from 0.64 to 1.00 (Figure S7c), suggesting a substantial response in leaf-level respiration to elevated temperature.

Vegetative heat tolerance can be predicted from novel coefficients extracted from segmented models of the F_v/F_m temperature response

To determine the efficiency of the coefficients extracted from the segmented models, i.e. T_{crit} and m_1, for forecasting heat tolerance, we compared the variation in these parameters obtained from juvenile leaf tissue to variation in heat tolerance parameters resulting from the heat-stress experiment performed on adult plants. m_1 demonstrated a tight positive correlation with SGR ($P = 0.02$; $R^2 = 0.72$; Figures 5 and 7c; Table S1), thereby suggesting that the genotypes in which the leaf tissue responds less strongly, in terms of F_v/F_m, to the initial incremental temperatures in the chlorophyll fluorescence assay were the same as those that demonstrated an enhanced maintenance of chlorophyll content and heat tolerance. Similarly, T_{crit} demonstrated a negative correlation with SGR ($P = 0.08$; $R^2 = 0.50$; Figures 5 and 7b; Table S1), highlighting that the genotypes that demonstrated the highest temperature breakpoint in the response of F_v/F_m to temperature were the most heat tolerant.

We also gauged heat tolerance in adult plants as the percentage reduction in ϕPSII from the first to the last day of the heat-stress period. The percentage reduction in ϕPSII was positively associated with SGR ($P = 0.08$; $R^2 = 0.50$; Figure 5; Table S1), suggesting a good level of agreement between the two metrics of heat tolerance. Moreover, the percentage reduction in ϕPSII was negatively correlated with T_{crit} ($P = 0.02$; $R^2 = 0.72$; Figure 5; Table S1), further highlighting the efficiency of T_{crit} for forecasting heat tolerance.

Daytime respiration (R_d) was the photo-physiological trait that demonstrated the greatest plasticity to heat stress (Figure S7c), indicating a role for respiration in heat tolerance. In concurrence, R_d after heat-stress initiation demonstrated a positive association with SGR ($P = 0.10$; $R^2 = 0.45$; Figure 5; Table S1). Furthermore, R_d after heat-stress initiation was positively associated with T_{crit} ($P = 0.01$; $R^2 = 0.76$; Figure 5; Table S1) and negatively associated with m_1 ($P = 0.07$; $R^2 = 0.40$; Figure 5; Table S1), suggesting that the lines forecast to have elevated heat tolerance had the most reduced rates of respiration during heat stress. Variation in R_d before the initiation of heat stress did not correlate with any of these aforementioned parameters, notwithstanding the lack of a G × T interaction, suggesting that R_d under optimal conditions is not a suitable indicator of future heat tolerance.

DISCUSSION

m_1 *and* m_2 as proxies of heat tolerance and heat resistance, respectively

Assessing heat tolerance across many genotypes is constrained by issues related to space for growing plants and facilities and equipment for experimentally increasing the temperature, both in controlled (Wang *et al.*, 2012) and field environments (Thomey *et al.*, 2019). Here we detail a rapid methodology for assaying heat tolerance that does not require substantial space to grow plants and that is correlated with independent estimates of heat tolerance in genetically diverse adult rice plants. The novel coefficients m_1 and T_{crit} represent high-throughput proxies for heat tolerance that can be used as specific targets for developing climate-resilient rice.

Photo-physiological screening of excised leaf material through chlorophyll fluorescence has recently been demonstrated to be equivalent to screening intact material (McAusland *et al.*, 2019), even over extended time periods (>3 h) similar to those employed in the present study. In addition, the lack of response in F_o and F_v/F_m to the experimental procedure performed without temperature changes (Figure S1a,b) suggests that the demonstrated responses observed for these parameters primarily result from the rapid incremental temperature changes (Figure 2a,b). In general, very few plant species exhibit deleterious effects on photosynthesis at temperatures below 30°C (Zhang and Sharkey, 2009), indeed the optimum temperature for rice cultivation can be as high as 35°C (Ghadirnezhad and Fallah, 2014). Indeed, the majority of the accessions studied here did not demonstrate substantial changes in F_v/F_m below 30°C (Figure 2b). Interestingly, IR 64 did show a reasonable response in this range, explainable in part by it being a *mega indica* variety developed in the Philippines, where quarterly average temperatures have never exceeded 27°C (Stuecker *et al.*, 2018). Conversely, the remaining accessions in this study are *aus indica* varieties from the Indian subcontinent that are typically cultivated during much warmer summer periods (Travis *et al.*, 2015). Furthermore, IR 64 has been demonstrated to be fairly susceptible to moderate temperature increases (Kilasi *et al.*, 2018). The heat tolerance of the *aus* varieties employed in this study have never previously been empirically tested.

The slow reduction in F_v/F_m up to T_{crit} can be used to assess the reduction in photosynthesis that can be considered manageable for maintaining growth and reversible upon the return of optimal temperatures (Crafts-Brandner and Salvucci, 2000; Sage and Kubien, 2007; Zhang and Sharkey, 2009). At these temperatures, reductions in photosynthesis result from reduced carbon metabolism and reduced electron transport. The reduction in carbon metabolism is primarily caused by decreased Rubisco activation (Perdomo *et al.*, 2017). The reduction in photosynthesis quantified by our rapid assay is caused by perturbed electron transport, however, in line with long-standing work that recognizes PSII as a heat-labile component of photosynthesis (Berry and Bjorkman, 1980; Williams *et al.*, 1985). More specifically, the initial reduction in F_v/F_m as a result of moderate temperatures (Figure 2b) can reflect an increase in the leakiness of thylakoid membranes (Havaux, 1996), which in turn accelerates photophosphorylation (Bukhov *et al.*, 1998), denoted here by the concurrent rise in F_o (Figure 2a) indicating a reduction in the plastoquinone pool. As PSII complexes are embedded in the lipid bilayers of thylakoid membranes, their functional efficiency is affected by the condition of the membranes. Under these moderate initial temperatures, however, thylakoid membranes can easily unfold and allow PSII repair machinery to access damaged protein complexes (Theis and Schroda, 2016; Yoshioka-Nishimura, 2016). For this reason, it is appropriate to consider m_1 as a metric of the adaptive photosynthetic response to temperature, as it represents the slope of the initial F_v/F_m response (Figure 2c). Genotypes with reduced m_1 can therefore be considered heat tolerant, as they are able to maintain close-to-optimal photosynthesis under heat stress.

As temperatures increase beyond the adaptive range, tolerating heat and maintaining close-to-optimal photosynthesis is no longer viable, and the response of F_v/F_m to temperature reflects the innate susceptibility of photosynthetic biochemistry to elevated temperatures. The T_{crit} parameter reflects this transition in response (Figure 2c). The response of F_v/F_m to temperatures beyond T_{crit} represents a sequence of well-characterized steps in heat-induced disassembly and denaturation of chlorophyll-containing protein complexes (Lípová *et al.*, 2010). For PSII complexes, this initially involves the release of the manganese-stabilizing protein perturbing the oxygen evolution reaction (Thompson *et al.*, 1989; Yu *et al.*, 2006), and

culminates in the formation of a complex that is non-fluorescent and cannot return to an active state (Satoh *et al.*, 1998). As m_2 represents the rapid response of F_v/F_m to temperature that occurs after moderate heat stress (Zhang and Sharkey, 2009), it can be considered a measure of the rate of deconstruction of PSII (Thompson *et al.*, 1989). To this end, lines that demonstrate reduced rates of m_2 can be considered heat resistant, which in this case is distinct from heat tolerance as benchmarked by m_1, in that it gauges the capacity to restrain permanent damage as opposed to maintaining typical plant function.

We observed an expected negative correlation between m_1 and T_{crit} (Figures 4d and 5; Table S1), which highlights how lines that are not able to tolerate moderate heat stress efficiently transition to the m_2 phase more rapidly. Conversely, m_2 was not correlated with T_{crit} (Figure 5; Table S1), which demonstrates that the temperature point at which leaf segments enter the rapid-response phase does not influence this secondary rate. Interestingly, we also observed a highly significant negative correlation between the two response phases (Figure 5; Table S1). This suggests that the lines with improved heat tolerance have reduced heat resistance. That is to say, the lines that are better equipped to maintain photosynthetic biochemistry under moderate heat stress are the same lines in which PSII protein complexes are disassembled more quickly following the transition to the rapid-response phase, i.e. m_2 and vice versa. As m_2 is not a function of T_{crit} (Figure 5; Table S1), the uncoupling of m_1 and m_2 is potentially related to the three-dimensional structure of thylakoid membranes within chloroplasts. Photoinhibition stimulated through increasing temperatures (Murata *et al.*, 2007) can be addressed by the PSII repair machinery. As noted previously, this repair system requires alterations to the thylakoid membrane, and consequently the PSII repair cycle and thylakoid membrane dynamics share a close relationship (Yoshioka-Nishimura, 2016). To this end, it is conceivable that membranal characteristics, e.g. curvature, thickness, stromal gaps, etc., that determine the ease of access to reversibly damaged PSII complexes under moderate heat stress, thus determining m_1, may also accelerate non-reversible protein complex damage after T_{crit}, thereby also defining m_2. This represents an interesting avenue for future research and crop improvement, as many of the genes that control these membranal characteristics have been elucidated (Fristedt *et al.*, 2009; Samole *et al.*, 2012; Armbruster *et al.*, 2013). Future work to this end could, for example, perform incremental temperature-response assays of thylakoid structure between wild-type lines and lines transformed to differentially express key genes involved in thylakoid membranal characteristics. Similarly, a key signal of moderate heat stress is the de-phosphorylation of important PSII component proteins (Sharkey 2005), and consequently it would also be highly interesting to determine how incremental temperature increases impact this de-phosphorylation, and whether this stimulates cyclic electron flow around PSI more in transgenic lines with altered thylakoid membrane structures than in wild-type lines.

It is important to note that previous work has adopted similar strategies to assess the temperature response of F_o and/or F_v/F_m (Schreiber and Berry, 1977; Lazár and Ilík, 1997; Xu *et al.*, 2014; Ribeiro *et al.*, 2015; Marias *et al.*, 2017); however, these studies were constrained by equipment issues, meaning at best only three species (Schreiber and Berry, 1977), genotypes (Xu *et al.*, 2014) or developmental stages (Marias *et al.*, 2017) were able to be compared in terms of their photosynthetic response to incrementally increasing temperatures. A fundamental aim of this present study was to determine the efficacy of the coefficients extracted from the segmented models for forecasting heat tolerance. As a result of the commonly encountered space constraints for performing heat experiments on adult plants, we limited the number of genotypes in this study to seven. Despite this, the experimental procedure to assay the response of chlorophyll fluorescence to incrementally increasing temperatures could easily be employed to screen >200 leaf segments at a time (McAusland *et al.*, 2019), thereby opening up the possibility of surveying large populations or many species. A further advance in this present study compared with the aforementioned studies is with respect to the determination of T_{crit} or its equivalent. In all cited studies, T_{crit} is calculated manually by the authors selecting the points that they best believe represent the slow and fast portions of the temperature-dependent response, fitting linear models to those points and determining where those models transect (Schreiber and Berry, 1977; Lazár and Ilík, 1997; Xu *et al.*, 2014; Ribeiro *et al.*, 2015; Marias *et al.*, 2017). Through this approach, these studies introduce substantial human bias in their calculation of T_{crit}. This bias is alleviated in our study through the broken-line analysis that computationally determines T_{crit} (Figure 2c). Furthermore, these cited studies do not attempt to characterize the linear portion of the models for any purpose, nor define their relevance.

m_1 and T_{crit} effectively forecast vegetative heat tolerance in adult rice plants

To determine the usefulness of the coefficients extracted from the segmented models for forecasting heat tolerance in adult plants, we subjected 60-day-old rice plants to a heat-stress period of 7 days (Figures 6, S2 and S3). At this point, all accessions were transitioning from the tillering to the stem elongation growth phase. This developmental timing was selected because of the importance of the SG phenotype at this stage for assessing abiotic stress tolerance, as it relates to the maintenance of photosynthesis and thus contributes to floral development and eventual

seed set and seed filling (Cossani and Reynolds, 2012; Jagadish *et al.*, 2015; Pinto *et al.*, 2016). SG is best defined as 'heritable delayed foliar senescence' (Thomas and Stoddart, 1975). It has been demonstrated to be a highly effective physical marker for chlorophyll content and has been used as a selection tool for crop breeding (Xu *et al.*, 2000; Cossani and Reynolds, 2012; Thomas and Ougham, 2014; Pinto *et al.*, 2016). We detected substantial variation in SGR 7 days after heat-stress initiation (Figure 7a). Our visual assessment of SGR follows on from those well-established and cited studies in providing low-variance estimates of senescence; however, we recommend that future work to characterize plant- or leaf-level senescence could be improved in throughput and objectivity through the development and adoption of software facilitating machine-based image assessments of SG. Multiple types of SG have been characterized in cereals and these can essentially be divided into two forms: cosmetic and functional. Cosmetic SG refers to the capacity to delay senescence without maintaining photosynthesis, in contrast to the functional form (Thomas and Howarth, 2000; Thomas and Ougham, 2014). The strong correlation between the percentage decline in ϕPSII and SGR demonstrates that the SG variation assessed in this study was of the functional form (Figure 5; Table S1). That is to say, the visual assessment of SG screened for the capacity to stabilize photosynthesis. This corroborates previous work in wheat that demonstrated strong links between SG, biomass accumulation and PSII efficiency (Sharma *et al.*, 2012, 2015; Sharma *et al.*, 2017).

Variation in SGR was associated with both T_{crit} (Figures 5, 7b, Table S1) and m_1 (Figures 5, 7c, Table S1), thereby demonstrating the effectiveness of these parameters determined from juvenile leaf segments for forecasting vegetative heat tolerance in adult plants. The negative association between T_{crit} and SGR (Figures 5 and 7b; Table S1) demonstrates that the lines that enter the rapid temperature response phase at higher temperatures also have improved vegetative heat tolerance as adult plants. As previously discussed, we interpret m_1 to be the most applicable predictor of heat tolerance, as it directly relates to the ability to maintain close-to-optimal photosynthetic biochemistry before heat resistance to restrain PSII disassembly becomes necessary as the heat stress intensifies. This is reflected by the variation in SGR being more explainable by variation in m_1 ($R^2 = 0.72$) than by variation in T_{crit} ($R^2 = 0.50$). Furthermore, we did not observe any association between m_2 and SGR or the percentage reduction in ϕPSII; this is probably because these gold-standard assessments performed on adult plants during heat stress quantify heat tolerance and not heat resistance. It is important to note that this study was limited to just seven accessions for determining the efficiency of m_1 as a proxy for heat tolerance. Despite this, we still demonstrated a very strong correlation between m_1 and SGR, and we propose that this minor limitation could be addressed in future studies that employ this methodology for screening diverse germplasm, such as mapping or mutagenized populations, through the selection of a set of accessions that fall along a wide range of m_1 values, and testing them for measured vegetative heat tolerance (SGR) for confirmation purposes. The assessment of such populations in this manner offers a clear strategy for future crop development via forward genetics and would also unequivocally confirm the efficiency of this methodology as a high-throughput phenotyping platform.

Respiration is more responsive to heat stress than photosynthetic capacity, and is linked to forecasted and measured heat tolerance

We measured the response of A_n to incrementally increasing c_i before and after heat-stress initiation in order to test the response of photosynthetic capacity to temperature (Figure 8a,b). From the A_n–c_i response measurements, we modelled V_{cmax} and J_{max} to gauge the efficiency of carboxylation by Rubisco and the rate of electron transport, respectively. These parameters are frequently assessed to determine the photo-physiological response to heat stress (Perdomo *et al.*, 2016; Haworth *et al.*, 2018; Thomey *et al.*, 2019; Chen *et al.*, 2019); however, we believe that this is the first instance of genetic variation in these parameters being tested under heat stress in rice in a substantial and genetically diverse set of lines. All accessions demonstrated a downregulation in V_{cmax} (Figure 8a), which is likely to be linked to Rubisco activase thermosensitivity (Feller *et al.*, 1998; Makino and Sage, 2007), as well the degradation of other Calvin-cycle enzymes (Sharkey, 2005) and general metabolic reprogramming in the chloroplasts (Wang *et al.*, 2018). Despite this, the observed reduction in the rate of consumption of RuBP by Rubisco did not appear to limit A_n (Figure S6b,c). This is in agreement with previous work that has demonstrated that when operating away from the thermal optimum, the capacity of Rubisco is not a rate-limiting factor for light-saturated CO_2 assimilation (Sharkey, 1985; Kubien and Sage, 2008). Curiously, in all but one of the seven accessions we observed a significant upregulation in J_{max} after heat-stress initiation, suggesting a substantial alteration to the energy sink balance. Under optimal conditions, the vast majority of energy is supplied to photosynthetic carbon reduction (Dani *et al.*, 2014); however, heat and other abiotic stressors can substantially alter this balance as the electron demand from non-photosynthetic processes, primarily elevated photorespiration (Noctor *et al.*, 2002) and isoprenoid emissions (Dani *et al.*, 2014), increases. To this end we calculated the ratio of J_{max} to V_{cmax} to determine the balance of electron transport to carboxylation events, and noted an increase in this ratio (Figure S6a) in response to heat stress, thereby

confirming an increase in non-photosynthetic electron demand and highlighting an adjustment in leaf nitrogen investments in response to temperature (Benomar *et al.*, 2019).

Reflecting the increased non-photosynthetic energy demand, we also observed a hugely significant upregulation in R_d, modelled as non-photorespiratory release of CO_2 from A_n–c_i response curves, in response to heat stress. Indeed, of all the photo-physiological traits measured pre- and post-heat stress initiation, R_d demonstrated by far the greatest degree of phenotypic plasticity in all accessions (Figure S7). It is worth noting, however, that the A_n–c_i response measurements of heat-stressed plants were performed 5 days after heat-stress initiation, which is before substantial reductions in ϕPSII were observed (Figures 6 and S3). Consequently, this demonstrates that at the leaf level, respiration appears to respond earlier to heat stress than photosynthetic processes. We propose that future work should seek to better understand how and why respiration responds earlier to heat stress in rice than photosynthesis does. This will allow for the determination of direct photo-physiological targets for mitigating heat stress perturbations. For example, diurnal measurements of dark respiration would elucidate the extent to which both nighttime and daytime respiration contribute to senescence and yield reductions. Additionally, more specific estimates of respiration, via gas-exchange measurements under low O_2 or via direct measurements of leaf level O_2 exchange, would allow for a higher resolution overview of natural variation in heat stress-induced respiration within diverse germplasm. For this reason, respiration may represent a more efficacious physical marker than photosynthesis for the early detection of heat-stress sensitivity. The upregulation of R_d here reflects our understanding of the temperature sensitivity of respiration (Kruse *et al.*, 2011; Gauthier *et al.*, 2014), which is a major limiting factor for ecosystem and agricultural productivity because it increases the percentage of fixed CO_2 that is re-released into the atmosphere, thereby reducing the portion of total photosynthates available for growth and productivity (Huntingford *et al.*, 2013). Indeed, leaf-level and whole-plant respiration have been attributed to substantial yield losses in rice (Mohammed and Tarpley, 2009) and other species (Nadeem *et al.*, 2018; Posch *et al.*, 2019). Reflecting the detrimental impact of heat-induced respiration on plant growth and productivity, we observed a positive association between R_d measured during heat stress and SGR, implying that the lines that demonstrated greater visual symptoms of senescence were respiring more. Furthermore, this association reflects the fact that senescence is a hugely energy-intensive process that requires substantial biochemical and metabolic reprogramming (O'Leary *et al.*, 2017). Interestingly, the m_1 and T_{crit} parameters were also significantly associated in the expected direction with R_d during heat stress, but not prior to heat stress, further highlighting the efficiency of these parameters for forecasting overall heat tolerance. Conversely, the variation in photosynthetic capacity assessed as V_{cmax} and J_{max} during heat stress was not associated with the percentage decline in ϕPSII or SGR.

Conclusion

In summary, this article details the development of a high-throughput phenotyping methodology for assessing the response of F_v/F_m to temperature and demonstrates the use of a novel modelling approach to characterize this response in terms of heat tolerance and heat resistance. Moreover, we have demonstrated that the coefficients extracted from these segmented models that pertain to heat tolerance represent accurate proxies of measured heat tolerance in adult plants. Additionally, our forecasting and assessment of adult heat tolerance was closely linked to daytime respiration, but not photosynthetic capacity, thereby highlighting the importance of non-photorespiratory CO_2 release as a target for developing heat tolerance in rice. A natural progression for this work is to employ this platform for forward genetics by screening populations of natural or induced genetic variants with the ultimate aim of elucidating genetic loci linked to heat tolerance. Similarly, this platform represents a strategy for varietal selection in a plant breeding context.

EXPERIMENTAL PROCEDURES

Plant material and growing conditions

A random selection of six genotypes from the Bengal and Assam Aus Panel (BAAP; Norton *et al.*, 2018) and the reference rice genotype IR 64 were selected for this study (Table 1). We had no prior information regarding the response of any of these genotypes to heat stress. Six biological repeats of each genotype were sown directly into a specialized rice compost (50:50; John Innes 3:Levington M3, The Scotts Company, Ipswich, UK). Prior to sowing, all seeds were heat treated to prevent fungal infection by submerging them in water within a 2.0-ml screwcap tube and heating them to 50°C for 40 min. Plants were initially sown just beneath the soil surface in 5-cm × 5-cm cell trays before being transplanted into 2-L pots filled with the same soil type 2 weeks after germination.

All plants were grown in the same GEN1000 reach-in growth chamber (Conviron, https://www.conviron.com) at the University of Nottingham in 2019. The growth chamber was set to a 12-h photoperiod (06:00–18:00 h) with the following conditions: 32°C day temperature, 27°C night temperature, 65% day relative humidity (RH) and 60% night RH. The light level was set to maximum, where the average light level above the plants increased from 600 to 1000 μmol m^{-2} photosynthetic photon flux density (PPFD) as the plants grew. On day 60 post sowing, when all plants were in the stem elongation growth stage, the day temperature of the growth chamber was increased to 42°C and the night temperature was increased to 37°C.

At 7 days after heat-stress initiation, the SG of five biological repeats of each genotype was scored via a visual rating system. Scoring used a scale from 1 to 5 based on the proportion of leaf

Table 1 List of genotypes used in this study. For each genotype, where applicable, ID codes corresponding to the Bengal and Assam Aus Panel (BAAP; Norton *et al.*, 2018), the International Rice Germplasm (IRGC) and Genetic Stocks Oryza (GSOR) collections are provided, along with the country of origin

Genotype	BAAP ID	IRGC ID	GSOR ID	Country of origin
BRRI 28	256	–	–	Bangladesh
Aus Kushi	111	66688	–	Bangladesh
BJI	200	–	301006	India
DJ 123	213	–	310307	Bangladesh
Pachodi 427	274	–	311589	India
Black Gora	201	–	301017	India
IR 64	285	117268	–	Philippines

area of normal sized leaves that had prematurely senesced or died. An SGR of 1 indicated no senescence, an SGR of 3 indicated approximately 50% leaf death and an SGR of 5 indicated complete leaf and stem death. This visual assessment of SG has been successfully employed for rice and has been shown to be highly correlated with chlorophyll content (Xu *et al.*, 2000; Jiang *et al.*, 2004; Hoang and Kobata, 2009).

Chlorophyll fluorescence

At 10 days post germination, a leaf segment approximately 8 mm × 20 mm was excised from the youngest leaf of five biological repeats of each genotype. Each leaf segment was placed on top of damp filter paper in a random order defined using a random list generator. The filter paper and leaf segments were then encased between glass plates (approx. 1 cm thick) on either side. Glass plates containing leaf segments (adaxial side up) were then arranged inside a closed 800C FluorCam chlorophyll fluorescence imager (Photon System Instruments, https://psi.cz). Leaf segments were dark adapted for 1 h before measurements. After dark adaptation, the standard F_v/F_m protocol of the associated FLUORCAM 7 software (Photon System Instruments) was run (McAusland *et al.*, 2019). Here, a measuring light pulse (PPFD 0.09 μmol m^{-2}) provides a measure of minimal chlorophyll fluorescence (F_o) and a follow-up saturating light pulse (PPFD 5500 μmol m^{-2}) provides a measure of maximum chlorophyll fluorescence (F_m). Variable fluorescence (F_v) is calculated as $F_m - F_o$ and the maximum quantum efficiency of PSII is calculated as F_v/F_m. All fluorescence parameters measured in this way were averaged across the entire leaf segment.

The initial measurements of F_v/F_m were performed at room temperature (approx. 21°C). Following this, the glass plates were removed from the closed chlorophyll fluorescence imager and the room was kept dark to maintain the dark-adapted states of the leaf segments. The glass plates were then placed inside sealed plastic bags. The sealed plastic bags were then placed into a water bath set to 25°C for 15 min. The plates were then removed from the water bath and plastic bags and re-positioned within the closed chlorophyll fluorescence imager. F_v/F_m was then measured again using the protocol described above. This process was then repeated at the following temperatures: 27.5, 30, 32, 34, 35, 37, 38, 39, 40, 42, 44, 46, 48 and 50°C. The only adjustment being the water bath incubation time, which was temperature dependent and selected based on the time taken for the leaf segments to reach the target temperature. The period of time needed to reach target temperature was defined by placing a thin-wire thermocouple next to leaf segments during protocol development. Sampling of leaf material occurred between 07:30 and 08:00 h. Dark adaptation of leaf material occurred between 08:15 and 09:15 h and the chlorophyll fluorescence measurements at the incremental temperatures occurred between 09:20 and 13:20 h.

To test whether the above protocol without any temperature changes initiated chlorophyll fluorescence responses, we performed the protocol exactly as above but without altering the water bath temperature until the final three steps, where it was changed to 30, 40 and 45°C. This testing was performed using five biological repeats of the IR 64 rice genotype.

To characterize the response of F_v/F_m to the incrementally increasing temperatures we employed segmented (or broken-line) relationships using the 'segmented()' function from the R package SEGMENTED (Muggeo, 2017). Initially, and for each individual leaf segment, a linear model is built where F_v/F_m is expressed as a function of temperature using the base 'lm()' function in R. The 'segmented()' function then estimates a new model based on the initial linear model. The new model is characterized by a segmented relationship through the introduction of breakpoint(s) based on changes in the relationship of F_v/F_m and temperature. Individual linear models are then fitted before and after any breakpoint(s). It is possible to define the approximate location and number of breakpoints; however, we opted against this to avoid introducing any human bias. Despite this, only one breakpoint was ever detected in all of the segmented models constructed. Three coefficients were extracted from each segmented model (Figure 2c): (i) the breakpoint or critical temperature of F_v/F_m (T_{crit}); (ii) the slope of the initial response of F_v/F_m to temperature before T_{crit} (m_1); and (iii) the slope of the secondary response of F_v/F_m to temperature after T_{crit} (m_2). The R code to generate segmented models across multiple independent F_v/F_m temperature responses is available at: github.com/johnferguson1989/tpj_paper_Ferguson2020.

Chlorophyll fluorescence measurements made during the adult heat-stress experiment were performed using a FluorPen portable fluorometer (Photon System Instruments). The 'QY' protocol was used to initially achieve a measure of steady-state fluorescence in light (F') via a measuring light pulse (PPFD 0.09 μmol m^{-2}). Subsequently, a measure of maximal fluorescence in light (F_m') was achieved through a saturating light pulse (3000 μmol m^{-2}). The operating efficiency of PSII photochemistry (ϕPSII) was then calculated as: $F_m' - F'/F_m'$. This protocol was performed on five biological repeats of each genotype every day during the heat-stress period. For each biological repeat ($n = 5$ per genotype), four technical repeat measurements of ϕPSII were performed on the youngest fully expanded leaf of the main tiller and then averaged. These measurements were performed between 12:00 and 13:00 h each day. We determined the percentage decrease in ϕPSII of all plants measured based on the ϕPSII values on day 0 and day 7 of the heat stress. These percentage decrease values were then averaged for each genotype.

Leaf gas exchange

Infra-red leaf level gas exchange was performed using three LI-6800 gas exchange systems (LI-COR, https://www.licor.com). To minimize time and instrument effects, the order of measurements and the system used for each plant was determined by a random list generator.

Initial gas-exchange chamber conditions were set as follows: 32°C heat-exchange temperature; 65% RH; 400 μmol mol^{-1} reference CO_2 concentration; and 1000 μmol $m^{-2}sec^{-1}$ PPFD. For the gas-exchange measurements performed 5 days after heat-stress initiation, the heat-exchange temperature was set to 42°C. The middle portion of the youngest fully expanded leaf of the main

tiller of each measured plant was selected for gas exchange. Once clamped on, the leaves were allowed to equilibrate to the chamber conditions, which typically took between 30 and 40 min. Upon stability, rates of photosynthesis (A_{400}) and stomatal conductance to water (g_s) were logged, from which the intrinsic water-use efficiency (*iWUE*) was calculated as A_{400}/g_s. Subsequently, an A_n–c_i response curve was initiated, where the reference CO_2 concentration was altered incrementally to the following steps: 300, 200, 100, 50, 400, 600, 800, 1000, 1200, 1400 and 1600 μmol mol^{-1}. At each incremental step, rates of gas exchange were allowed to stabilize for a minimum of 90 sec and a maximum of 120 sec according to standard error stability criteria based on g_s and A_n. A_n at the final A_n–c_i step was logged as A_{max}. These measurements were performed between 08:00 and 15:00 h 3 days before heat-stress initiation and 5 days after heat-stress initiation. Between four and six biological repeats of each genotype were measured.

The photosynthesis model of Farquhar *et al.* (1980) was fitted to all A_n–c_i response curves using the bilinear method of the 'fitacis()' function from the R package PLANTECOPHYS (Duursma, 2015). This fitting method provides estimates of Rubisco carboxylation capacity (V_{cmax}), potential electron transport rate (J_{max}) and daytime respiration (R_d, also referred to as the non-photorespiratory CO_2 release rate). We also calculated the ratio J_{max}:V_{cmax}. The 'photosyn()' function from PLANTECOPHYS was used to obtain photosynthesis model estimates of A_n from 50 to 1000 c_i for visualization purposes.

The phenotypic plasticity of photosynthesis-related traits to heat stress was calculated according to the PPI (Valladares *et al.*, 2006). Here, the mean values for each photosynthetic trait of each genotype 3 days before and 5 days after heat-stress initiation was used to calculate plasticity as: (maximum mean − minimum mean)/maximum mean.

A glossary of all chlorophyll fluorescence and leaf gas-exchange parameters measured and modelled in this study can be found in Table 2.

Statistical analyses

All data processing, analyses and figure generation were performed within the R software environment (R Core Team, 2014). Additional post-processing of figures was performed in AFFINITY DESIGNER (Serif, https://www.serif.com).

A repeated-measures two-way analysis of variance (ANOVA) was performed to determine the effect of genotype and temperature, and their interaction, on F_o and F_v/F_m. This was achieved using the 'anova_test()' function from the RSTATIX package.

To determine the effectiveness of the segmented model approach for characterizing the response of F_v/F_m to temperature, we additionally characterized this response through linear and quadratic models. For each individual biological repeat, the coefficient of determination (R^2) of the segmented, linear and quadratic models was extracted. All models were fitted using the base 'lm()' function in R. One-way ANOVA comparison of means testing was used to determine whether there were significant genotype effects on the R^2 value for all three model types using the base 'aov()' function in R.

For all measured traits, except ϕPSII (on all days measured), a single one-way ANOVA was performed to determine whether there were significant genotype effects for traits of interest. Subsequently, post-hoc Tukey tests were performed to facilitate multiple comparisons between genotypes. Post-hoc Tukey tests were performed using the 'HSD.Test()' function from the R package AGRICOLAE (Mendiburu *et al.*, 2015), with the alpha significance threshold being set to 0.10. For the traits measured through infra-red gas analysis, a three-way ANOVA was initially performed to determine whether the LI-6800 instrument used and the hour the measurement was performed, as well as genotype, had a significant effect on the trait of interest. Neither instrument nor hour of measurement were observed to have a noticeable effect on any measured trait ($P > 0.05$). In addition, and to test for genotype × treatment (G × T) interactions for the photophysiological traits measured before and after heat-stress initiation, a two-way ANOVA with an interaction term was performed for all traits.

To test for associations between putative dependent and explanatory variables, e.g. SGR and T_{crit} (Figure 7a), or ϕPSII and days following heat-stress initiation (Figures 6a and S3), linear models were fitted. To more generally determine the existence of trait associations, tests for associations between paired samples using the Pearson's product–moment correlation coefficient were performed for all pairwise trait interactions using the 'rcorr()' function from the R package HMISC, which was subsequently visualized using the 'corrplot()' function from the R package CORRPLOT (McKenna *et al.*, 2016).

Table 2 Glossary of physiological parameters measured in this study

Trait	Units	Description
F_v/F_m	Dimensionless ratio	Maximum quantum efficiency of photosystem II (PSII)
F_o	Arbitrary	Minimum chlorophyll fluorescence
T_{crit}	°C	Critical temperature point for F_v/F_m, as determined by the segmented analyses
m_1	Slope of regression (m)	Slope of linear response of F_v/F_m to temperature before T_{crit}
m_2	Slope of regression (m)	Slope of linear response of F_v/F_m to temperature after T_{crit}
SGR	Arbitrary	Visual stay-green rating
ΦPSII	Dimensionless ratio	Apparent efficiency of PSII
V_{cmax}	μmol CO_2 m^{-2} sec^{-1}	Maximum carboxylation efficiency of Rubisco
J_{max}	μmol electrons m^{-2} sec^{-1}	Maximum electron transport rate
R_d	μmol CO_2 m^{-2} sec^{-1}	Day respiration
J_{max}/V_{cmax}	μmol electrons μmol $CO_2{}^{-1}$	Ratio of J_{max} to V_{cmax}
A_n	μmol CO_2 m^{-2} sec^{-1}	Net photosynthetic rate
A_{400}	μmol CO_2 m^{-2} sec^{-1}	Light-saturated net photosynthetic rate at ambient CO_2
A_{max}	μmo CO_2 m^{-2} sec^{-1}	Light-saturated net photosynthetic rate at CO_2 saturation
g_s	mol H_2O m^{-2} sec^{-1}	Light-saturated rate of stomatal conductance to water at ambient CO_2
iWUE	μmol CO_2 mol H_2O^{-1}	Intrinsic water-use efficiency, calculated as the ratio of A_{400} to g_s

DATA AVAILABILITY STATEMENT

Data included in this paper are available at github.com/johnferguson1989/tpj_paper_Ferguson2020.

ACKNOWLEDGEMENTS

We are grateful to the University of Nottingham glasshouse staff for their assistance with general plant maintenance. We thank Laura Briers for supplying the photograph used in Figure 1. This article benefited substantially from the critical insight of Dr Alex Burgess. JNF is supported by the Palaeobenchmarking Resilient Agriculture Systems (PalaeoRAS) project funded by the Future Food Beacon of the University of Nottingham. EHM receives funding from the Biotechnology and Biological Sciences Research Council (BBSRC, grant no. BB/R004633/1). KES is supported by a University of Nottingham–BBSRC Doctoral Training Partnership studentship.

AUTHOR CONTRIBUTIONS

JNF, LM, AHP, ZAW and EHM conceived and designed the study. AHP provided the germplasm. JNF, LM and KES performed the experiments. JNF analysed the data. JNF wrote the article, with input from all of the authors.

CONFLICT OF INTEREST

The authors declare no conflicts of interest.

SUPPORTING INFORMATION

Additional Supporting Information may be found in the online version of this article.

Figure S1. Response of F_o and F_v/F_m to consistent temperatures.

Figure S2. Photographs of representative plants after heat stress.

Figure S3. ϕPSII response to heat stress.

Figure S4. Variation in photosynthetic parameters before heat-stress initiation.

Figure S5. Variation in photosynthetic parameters after heat-stress initiation.

Figure S6. Interaction plots of genotype-specific heat-stress responses.

Figure S7. Photo-physiological plasticity to heat stress.

Table S1. Pairwise trait correlation matrix.

REFERENCES

Allakhverdiev, S.I., Kreslavski, V.D., Klimov, V.V., Los, D.A., Carpentier, R. and Mohanty, P. (2008) Heat stress: an overview of molecular responses in photosynthesis. *Photosynth. Res.* **98**, 541–550.

Armbruster, U., Labs, M., Pribil, M. *et al.* (2013) Arabidopsis CURVATURE THYLAKOID1 proteins modify thylakoid architecture by inducing membrane curvature. *Plant Cell*, **25**, 2661–2678.

Baker, N.R. (2008) Chlorophyll fluorescence: a probe of photosynthesis in vivo. *Annu. Rev. Plant Biol.* **59**, 89–113.

Benomar, L., Moutaoufik, M.T., Elferjani, R., Isabel, N., DesRochers, A., El Guellab, A., Khlifa, R. and Idrissi Hassania, L.A. (2019) Thermal acclimation of photosynthetic activity and RuBisCO content in two hybrid poplar clones. *PLoS One*, **14**, e0206021.

Berry, J. and Bjorkman, O. (1980) Photosynthetic response and adaptation to temperature in higher plants. *Annu. Rev. Plant Physiol.* **31**(1), 491–543.

Blum, A. (2009) Effective use of water (EUW) and not water-use efficiency (WUE) is the target of crop yield improvement under drought stress. *Field Crops Res.* **112**(2-3), 119–123. https://doi.org/10.1016/j.fcr.2009.03.009

Bukhov, N.G., Boucher, N. and Carpentier, R. Loss of the precise control of photosynthesis and increased yield of non-radiative dissipation of excitation energy after mild heat treatment of barley leaves. *Physiol. Plant.* **104**(4), 563–570. https://doi.org/10.1034/j.1399-3054.1998.1040407.x

Chaturvedi, A.K., Bahuguna, R.N., Shah, D., Pal, M. and Krishna Jagadish, S.V. (2017) High temperature stress during flowering and grain filling offsets beneficial impact of elevated CO2 on assimilate partitioning and sink-strength in rice. *Sci. Rep.* **7**(1), https://doi.org/10.1038/s41598-017-07464-6

Chen, S., Guo, Y., Sirault, X. *et al.* (2019) Nondestructive phenomic tools for the prediction of heat and drought tolerance at anthesis in brassica species. *Plant Phenomics*, **2019**, 1–16. https://doi.org/10.34133/2019/3264872

Cossani, C.M. and Reynolds, M.P. (2012) Physiological traits for improving heat tolerance in wheat. *Plant Physiol.* **160**, 1710–1718.

Crafts-Brandner, S.J. and Salvucci, M.E. (2000) Rubisco activase constrains the photosynthetic potential of leaves at high temperature and CO2. *Proc. Natl. Acad. Sci. U.S.A.*, **97**, 13430–13435.

Dani, K.G.S., Jamie, I.M., Prentice, I.C. and Atwell, B.J. (2014) Increased ratio of electron transport to net assimilation rate supports elevated isoprenoid emission rate in eucalypts under drought. *Plant Physiol.* **166**, 1059–1072.

Driedonks, N., Rieu, I. and Vriezen, W.H. (2016) Breeding for plant heat tolerance at vegetative and reproductive stages. *Plant Reprod.* **29**, 67–79.

Duursma, R.A. (2015) Plantecophys–an R package for analysing and modelling leaf gas exchange data. *PLoS One*, **10**, e0143346.

Farquhar, G.D., von Caemmerer, S. and Berry, J.A. (1980) A biochemical model of photosynthetic CO2 assimilation in leaves of C3 species. *Planta*, **149**(1), 78–90. https://doi.org/10.1007/BF00386231

Feller, U., Crafts-Brandner, S.J. and Salvucci, M.E. (1998) moderately high temperatures inhibit ribulose-1,5-bisphosphate carboxylase/oxygenase (Rubisco) activase-mediated activation of rubisco. *Plant Physiol.* **116**, 539–546.

Fristedt, R., Willig, A., Granath, P., Crèvecoeur, M., Rochaix, J.-D. and Vener, A.V. (2009) Phosphorylation of photosystem II controls functional macroscopic folding of photosynthetic membranes in Arabidopsis. *Plant Cell*, **21**, 3950–3964.

Fu, J.-D., Yan, Y.-F., Kim, M.Y., Lee, S.-H. and Lee, B.-W. (2011) Population-specific quantitative trait loci mapping for functional stay-green trait in rice (Oryza sativa L.). *Genome*, **54**, 235–243.

Gauthier, P.P.G., Crous, K.Y., Ayub, G. *et al.* (2014) Drought increases heat tolerance of leaf respiration in Eucalyptus globulus saplings grown under both ambient and elevated atmospheric [CO2] and temperature. *J. Exp. Bot.* **65**, 6471–6485.

Ghadirnezhad, R. and Fallah, A. (2014) Temperature effect on yield and yield components of different rice cultivars in flowering stage. *Int. J. Agron.* **2014**, 1–4. https://doi.org/10.1155/2014/846707

Havaux, M. (1996) Short-term responses of Photosystem I to heat stress: induction of a PS II-independent electron transport through PS I fed by stromal components. *Photosynth. Res.* **47**, 85–97.

Haworth, M., Marino, G., Brunetti, C., Killi, D., De Carlo, A. and Centritto, M. (2018) The impact of heat stress and water deficit on the photosynthetic and stomatal physiology of olive (Olea europaea L.)—a case study of the 2017 heat wave. *Plants*, **7**(4), 76. https://doi.org/10.3390/plants7040076

Hoang, T.B. and Kobata, T. (2009) Stay-Green in rice (Oryza sativa L.) of drought-prone areas in desiccated soils. *Plant Prod. Sci.* **12**, 397–408. https://doi.org/10.1626/pps.12.397

Huntingford, C., Zelazowski, P., Galbraith, D. *et al.* (2013) Simulated resilience of tropical rainforests to CO2-induced climate change. *Nat. Geosc.* **6** (4), 268–273. https://doi.org/10.1038/ngeo1741

IPPC. (2007) Climate Change 2007: The Physical Science Basis. In *Contribution of Working Group I to the Fourth Assessment Report of the Intergovernmental Panel on Climate Change* (Solomon, S., Qin, D., Manning, M., Chen, Z., Marquis, M., Averyt, K.B., Tignor, M. & Miller, H.L., eds). Cambridge, UK and New York, NY: Cambridge University Press. https://archive.ipcc.ch/report/ar4/

Jagadish, K.S.V., Kavi Kishor, P.B., Bahuguna, R.N., von Wirén, N. and Sreenivasulu, N. (2015) Staying alive or going to die during terminal senescence—an Enigma surrounding yield stability. *Front. Plant Sci.* **6**, 1070. https://doi.org/10.3389/fpls.2015.01070

Jajic, I., Sarna, T. and Strzalka, K. (2015) Senescence, stress, and reactive oxygen species. *Plants*, **4**(3), 393–411. https://doi.org/10.3390/plants4030393

Jiang, G.H., He, Y.Q., Xu, C.G., Li, X.H. and Zhang, Q. (2004) The genetic basis of stay-green in rice analyzed in a population of doubled haploid lines derived from an indica by japonica cross. *Theor. Appl. Genet.* **108** (4), 688–698. https://doi.org/10.1007/s00122-003-1465-z

Khanna-Chopra, R. (2012) Leaf senescence and abiotic stresses share reactive oxygen species-mediated chloroplast degradation. *Protoplasma*, **249**, 469–481.

Kilasi, N.L., Singh, J., Vallejos, C.E., Ye, C., Jagadish, S.V.K., Kusolwa, P. and Rathinasabapathi, B. (2018) Heat stress tolerance in Rice (L.): identification of quantitative trait loci and candidate genes for seedling growth under heat stress. *Front. Plant Sci.* **9**, 1578.

Kruse, J., Rennenberg, H. and Adams, M.A. (2011) Steps towards a mechanistic understanding of respiratory temperature responses. *New Phytol.* **189**, 659–677.

Kubien, D.S. and Sage, R.F. (2008) The temperature response of photosynthesis and metabolites in Anti-RbcS tobacco. In *Photosynthesis. Energy from the Sun* (Allen, J.F., Gantt, E., Golbeck, J.H. and Osmond, B., eds). Dordrecht: Springer, pp. 857–861. https://doi.org/10.1007/978-1-4020-6709-9_190

Kumar, U., Joshi, A.K., Kumari, M., Paliwal, R., Kumar, S. and Röder, M.S. (2010) Identification of QTLs for stay green trait in wheat (Triticum aestivum L.) in the "Chirya 3" × "Sonalika" population. *Euphytica*, **174**, 437–445. https://doi.org/10.1007/s10681-010-0155-6

Lancashire, P.D., Bleiholder, H., Van den Boom, T., Langelüddeke, P., Stauss, R., Weber, E. and Witzenberger, A. (1991) A uniform decimal code for growth stages of crops and weeds. *Ann. Appl. Biol.* **119**(3), 561–601. https://doi.org/10.1111/j.1744-7348.1991.tb04895.x

Lazár, D. and Ilík, P. (1997) High-temperature induced chlorophyll fluorescence changes in barley leaves Comparison of the critical temperatures determined from fluorescence induction and from fluorescence temperature curve. *Plant Sci.*, **124**(2), 159–164. https://doi.org/10.1016/S0168-9452(97)04602-5

Lim, P.O., Kim, H.J. and Nam, H.G. (2007) Leaf senescence. *Annu. Rev. Plant Biol.* **58**(1), 115–136. https://doi.org/10.1146/annurev.arplant.57.032905.105316

Lípová, L., Krchnák, P., Komenda, J. and Ilík, P. (2010) Heat-induced disassembly and degradation of chlorophyll-containing protein complexes in vivo. *Biochim. Biophys. Acta*, **1797**, 63–70.

Makino, A. and Sage, R.F. (2007) Temperature response of photosynthesis in transgenic rice transformed with "sense" or "antisense" rbcS. *Plant Cell Physiol.* **48**, 1472–1483.

Marias, D.E., Meinzer, F.C. and Still, C. (2017) Leaf age and methodology impact assessments of thermotolerance of Coffea arabica. *Trees*, **31**(3), 1091–1099. https://doi.org/10.1007/s00468-016-1476-4

McAusland, L., Atkinson, J.A., Lawson, T. and Murchie, E.H. (2019) High throughput procedure utilising chlorophyll fluorescence imaging to phenotype dynamic photosynthesis and photoprotection in leaves under controlled gaseous conditions. *Plant Methods*, **15**, 109.

McKenna, S., Meyer, M., Gregg, C. and Gerber, S. (2016) s-CorrPlot: an interactive scatterplot for exploring correlation. *J. Comput. Graph. Stat.* **25**(2), 445–463. https://doi.org/10.1080/10618600.2015.1021926

Mendiburu, F.D., De Mendiburu, F. and Simon, R. (2015) Agricolae - Ten years of an open source statistical tool for experiments in breeding, agriculture and biology. *PeerJ.* https://doi.org/10.7287/peerj.preprints.1404v1

Mohammed, A.-R. and Tarpley, L. (2009) Impact of high nighttime temperature on respiration, membrane stability, antioxidant capacity, and yield of rice plants. *Crop Sci.* **49**(1), 313–322. https://doi.org/10.2135/cropsci2008.03.0161

Muggeo, V.M.R. (2017) Interval estimation for the breakpoint in segmented regression: a smoothed score-based approach. *Aust. N. Z. J. Stat.* **59**(3), 311–322. https://doi.org/10.1111/anzs.12200

Murata, N., Takahashi, S., Nishiyama, Y. and Allakhverdiev, S.I. (2007) Photoinhibition of photosystem II under environmental stress. *Biochim. Biophys. Acta Bioenerg.* **1767**(6), 414–421. https://doi.org/10.1016/j.bbabio.2006.11.019

Murchie, E.H., Kefauver, S., Araus, J.L., Muller, O., Rascher, U., Flood, P.J. and Lawson, T. (2018) Measuring the dynamic photosynthome. *Ann. Bot.* **122**, 207–220.

Nadeem, M., Li, J., Wang, M., Shah, L., Lu, S., Wang, X. and Ma, C. (2018) Unraveling field crops sensitivity to heat stress: mechanisms, approaches, and future prospects. *Agronomy*, **8**(7), 128. https://doi.org/10.3390/agronomy8070128

Noctor, G., Veljovic-Jovanovic, S., Driscoll, S., Novitskaya, L. and Foyer, C.H. (2002) Drought and oxidative load in the leaves of C3 plants: a predominant role for photorespiration? *Ann. Bot.* **89**(7), 841–850. https://doi.org/10.1093/aob/mcf096

Norton, G.J., Travis, A.J., Douglas, A. *et al.* (2018) Genome Wide Association Mapping Of Grain And Straw Biomass Traits in the Rice Bengal and Assam Aus Panel (BAAP) grown under alternate wetting and drying and permanently flooded irrigation. *Front. Plant Sci.* **9**, 1223.

O'Leary, B.M., Lee, C.P., Atkin, O.K., Cheng, R., Brown, T.B. and Millar, A.H. (2017) Variation in leaf respiration rates at night correlates with carbohydrate and amino acid supply. *Plant Physiol.* **174**, 2261–2273.

Perdomo, J.A., Capó-Bauçà, S., Carmo-Silva, E. and Galmés, J. (2017) Rubisco and rubisco activase play an important role in the biochemical limitations of photosynthesis in rice, wheat, and maize under high temperature and water deficit. *Front. Plant Sci.* **8**, 490.

Perdomo, J.A., Carmo-Silva, E., Hermida-Carrera, C., Flexas, J. and Galmés, J. (2016) Acclimation of biochemical and diffusive components of photosynthesis in rice, wheat, and maize to heat and water deficit: implications for modeling photosynthesis. *Front. Plant Sci.* **7**, 1719.

Pinto, R.S., Lopes, M.S., Collins, N.C. and Reynolds, M.P. (2016) Modelling and genetic dissection of staygreen under heat stress. *Theor. Appl. Genet.* **129**, 2055–2074.

Posch, B.C., Kariyawasam, B.C., Bramley, H., Coast, O., Richards, R.A., Reynolds, M.P., Trethowan, R. and Atkin, O.K. (2019) Exploring high temperature responses of photosynthesis and respiration to improve heat tolerance in wheat. *J. Exp. Bot.* **70**, 5051–5069.

Rama Reddy, N.R., Ragimasalawada, M., Sabbavarapu, M.M., Nadoor, S. and Patil, J.V. (2014) Detection and validation of stay-green QTL in post-rainy sorghum involving widely adapted cultivar, M35–1 and a popular stay-green genotype B35. *BMC Genom.* **15**, 909.

R Core Team. (2014) *R: A language and environment for statistical computing: R Foundation for Statistical Computing*. Available at: http://www.R-project.org/

Ribeiro, R.V., dos Santos, M.G., Pimentel, C., Machado, E.C. and de Oliveira, R.F. (2015) Can the critical temperature for photochemical damage in common bean plants be changed after a drought event? *Bragantia*, **74**(4), 374–378. https://doi.org/10.1590/1678-4499.0141

Sage, R.F. and Kubien, D.S. (2007) The temperature response of C3 and C4 photosynthesis. *Plant Cell Environ.* **30**, 1086–1106. https://doi.org/10.1111/j.1365-3040.2007.01682.x

Samol I., Shapiguzov A., Ingelsson B., Fucile G., Crèvecoeur M., Vener Alexander V., Rochaix J.-D., Goldschmidt-Clermont M. (2012) Identification of a Photosystem II Phosphatase Involved in Light Acclimation in Arabidopsis. *The Plant Cell*, **24**(6), 2596–2609. http://dx.doi.org/10.1105/tpc.112.095703

Satoh, K., Yamane, Y., Emi, T., Kashino, Y. and Koike, H. (1998) Effects of high temperatures on photosynthetic systems: fluorescence Fo increases in cyanobacteria. *Photosynthesis: Mechanisms and Effects*, **1-V**, 2469–2472. https://doi.org/10.1007/978-94-011-3953-3_578

Schreiber, U. and Berry, J.A. (1977) Heat-induced changes of chlorophyll fluorescence in intact leaves correlated with damage of the photosynthetic apparatus. *Planta*, **136**, 233–238.

Sekhon, R.S., Saski, C., Kumar, R. *et al.* (2019) Integrated genome-scale analysis identifies novel genes and networks underlying senescence in maize. *Plant Cell*, **31**, 1968–1989.

Sharkey, T.D. (2005) Effects of moderate heat stress on photosynthesis: importance of thylakoid reactions, rubisco deactivation, reactive oxygen species, and thermotolerance provided by isoprene. *Plant Cell Environ.* **28**(3), 269–277. https://doi.org/10.1111/j.1365-3040.2005.01324.x

Sharkey, T.D. (1985) Photosynthesis in intact leaves of C3 plants: physics, physiology and rate limitations. *Bot. Rev.* **51**(1), 53–105. https://doi.org/10.1007/BF02861058

Sharma, D.K., Andersen, S.B., Ottosen, C.-O. and Rosenqvist, E. (2012) Phenotyping of wheat cultivars for heat tolerance using chlorophyll a fluorescence. *Funct. Plant Biol.* **39**(11), 936–https://doi.org/10.1071/FP12100

Sharma, D.K., Andersen, S.B., Ottosen, C.-O. and Rosenqvist, E. (2015) Wheat cultivars selected for high Fv/Fmunder heat stress maintain high photosynthesis, total chlorophyll, stomatal conductance, transpiration

and dry matter. *Physiol. Plant.* **153**, 284–298. https://doi.org/10.1111/ppl.12245

Sharma, D.K., Torp, A.M., Rosenqvist, E., Ottosen, C.-O. and Andersen, S.B. (2017) QTLs and potential candidate genes for heat stress tolerance identified from the mapping populations specifically segregating for /in wheat. *Front. Plant Sci.* **8**, 1668.

Sinvany-Villalobo, G., Davydov, O., Ben-Ari, G., Zaltsman, A., Raskind, A. and Adam, Z. (2004) Expression in multigene families. Analysis of chloroplast and mitochondrial proteases. *Plant Physiol.* **135**(3), 1336–1345. https://doi.org/10.1104/pp.104.043299

Stuecker, M.F., Tigchelaar, M. and Kantar, M.B. (2018) Climate variability impacts on rice production in the Philippines. *PLoS One*, **13**, e0201426.

Theis, J. and Schroda, M. (2016) Revisiting the photosystem II repair cycle. *Plant Signal. Behav.* **11**, e1218587.

Thomas, H. and Howarth, C.J. (2000) Five ways to stay green. *J. Exp. Bot.* **51**(Suppl 1), 329–337. https://doi.org/10.1093/jexbot/51.suppl_1.329

Thomas, H. and Ougham, H. (2014) The stay-green trait. *J. Exp. Bot.* **65**, 3889–3900.

Thomas, H. and Stoddart, J.L. (1975) Separation of chlorophyll degradation from other senescence processes in leaves of a mutant genotype of Meadow Fescue (*Festuca pratensis* L.). *Plant Physiol.* **56**, 438–441.

Thomey, M.L., Slattery, R.A., Köhler, I.H., Bernacchi, C.J. and Ort, D.R. (2019) Yield response of field-grown soybean exposed to heat waves under current and elevated [CO]. *Glob. Chang. Biol.* **25**, 4352–4368.

Thompson, L.K., Blaylock, R., Sturtevant, J.M. and Brudvig, G.W. (1989) Molecular basis of the heat denaturation of photosystem II. *Biochemistry*, **28**, 6686–6695.

Travis, A.J., Norton, G.J., Datta, S. *et al.* (2015) Assessing the genetic diversity of rice originating from Bangladesh, Assam and West Bengal. *Rice*, **8**, 35.

Uauy, C., Distelfeld, A., Fahima, T., Blechl, A. and Dubcovsky, J. (2006) A NAC Gene regulating senescence improves grain protein, zinc, and iron content in wheat. *Science*, **314**, 1298–1301.

Valladares, F., Sanchez-Gomez, D. and Zavala, M.A. (2006) Quantitative estimation of phenotypic plasticity: bridging the gap between the evolutionary concept and its ecological applications. *J. Ecol.* **94**(6), 1103–1116. https://doi.org/10.1111/j.1365-2745.2006.01176.x

Vijayalakshmi, K., Fritz, A.K., Paulsen, G.M., Bai, G., Pandravada, S. and Gill, B.S. (2010) Modeling and mapping QTL for senescence-related traits in winter wheat under high temperature. *Mol. Breed.* **26**(2), 163–175. https://doi.org/10.1007/s11032-009-9366-8

Wang, D., Heckathorn, S.A., Wang, X. and Philpott, S.M. (2012) A meta-analysis of plant physiological and growth responses to temperature and elevated CO2. *Oecologia*, **169**(1), 1–13. https://doi.org/10.1007/s00442-011-2172-0

Wang, Q.-L., Chen, J.-H., He, N.-Y. and Guo, F.-Q. (2018) Metabolic reprogramming in chloroplasts under heat stress in plants. *Int. J. Mol. Sci.* **19**(3), 849. https://doi.org/10.3390/ijms19030849

Williams, W.P., Thomas, P.G. and Quinn, P.J. (1985) Cryoinjury of membranes. *Cryobiology*, **22**(6), 637–https://doi.org/10.1016/0011-2240(85)90137-3

Xu, H., Liu, G., Liu, G., Yan, B., Duan, W., Wang, L. and Li, S. (2014) Comparison of investigation methods of heat injury in grapevine (Vitis) and assessment to heat tolerance in different cultivars and species. *BMC Plant Biol.* **14**, 156.

Xu, W., Rosenow, D.T. and Nguyen, H.T. (2000) Stay green trait in grain sorghum: relationship between visual rating and leaf chlorophyll concentration. *Plant Breed.* **119**(4), 365–367. https://doi.org/10.1046/j.1439-0523.2000.00506.x

Yoo, S.-C., Cho, S.-H., Zhang, H. *et al.* (2007) Quantitative trait loci associated with functional stay-green SNU-SG1 in rice. *Mol. Cells*, **24**, 83–94.

Yoshioka-Nishimura, M. (2016) Close relationships between the PSII repair cycle and thylakoid membrane dynamics. *Plant Cell Physiol.* **57**(6), 1115–1122. https://doi.org/10.1093/pcp/pcw050

Yu, H., Xu, X. and David Britt, R. (2006) The 33 kDa Protein Can Be Removed without Affecting the Association of the 23 and 17 kDa Proteins with the Luminal Side of PS II of Spinach†. *Biochemistry*, **45**, 3404–3411. https://doi.org/10.1021/bi051604o

Zhang, R. and Sharkey, T.D. (2009) Photosynthetic electron transport and proton flux under moderate heat stress. *Photosynth. Res.* **100**, 29–43.

Zhao, C., Liu, B., Piao, S. *et al.* (2017) Temperature increase reduces global yields of major crops in four independent estimates. *Proc. Natl. Acad. Sci. USA*, **114**, 9326–9331.

Zhu, X.-G., Long, S.P. and Ort, D.R. (2010) Improving photosynthetic efficiency for greater yield. *Annu. Rev. Plant Biol.* **61**, 235–261.